Controlling enhancement and suppression of four-wave mixing via polarized light

Changbiao Li,[1] Yanpeng Zhang,[1,*] Zhiqiang Nie,[1] Yigang Du,[1] Ruimin Wang,[1] Jianping Song,[1] and Min Xiao[2,†]

[1]*Key Laboratory for Physical Electronics and Devices of the Ministry of Education & Shaanxi Key Lab of Information Photonic Technique, Xi'an Jiaotong University, Xi'an 710049, People's Republic of China*

[2]*Department of Physics, University of Arkansas, Fayetteville, Arkansas 72701, USA*

(Received 12 November 2009; published 4 March 2010)

We show that the four-wave mixing (FWM) processes in a multi-Zeeman level atomic system can be enhanced and suppressed by changing the polarization of one of the pump beams. Different polarization states of the pump beams will act on different transition pathways among the multi-Zeeman levels with different transition strengths, which affect the FWM efficiencies. An additional dress field applied to the adjacent transition can cause energy level splitting and therefore control the enhancement and suppression of the FWM processes in the system. The experimental results are in good agreement with our theoretical calculations.

DOI: 10.1103/PhysRevA.81.033801 PACS number(s): 42.50.Gy, 42.65.Ky

I. INTRODUCTION

Polarizations of the involved laser beams can play important roles in electromagnetically induced transparency (EIT) [1–3] and four-wave mixing (FWM) processes [4–7] when multi-Zeeman energy levels are involved in the atomic systems [8,9]. Several previous experimental and theoretical studies have shown that EIT and FWM processes can be effectively controlled by selecting different transitions among Zeeman sublevels via the polarization states of the laser beams [3,7,8]. Also, additional dressing laser beams can modify the FWM efficiencies in multilevel atomic systems. In our previous experiments, we have shown the enhancement and suppression of FWM by controlling the dressing laser beams in the multilevel atomic systems [10].

In this article, we experimentally demonstrate that the degenerate FWM (DFWM) caused by two strong pumping beams and a weak probe beam in a two-level Zeeman-degenerate atomic system can be modified by the polarization states of the two pumping beams, and by an additional dressing beam interacting with an adjacent atomic transition, as shown in Fig. 1(a). The DFWM process is enhanced or suppressed due to the combined polarization and dressing effects. The polarizations of the pumping beams select the transitions among different Zeeman levels, which usually have different transition strengths [7], and the dressing beam determines the effective frequency detunings of the probe beam from the multi-Zeeman levels. The experimental observations clearly show the evolution of the DFWM enhancement and suppression versus pump field polarizations.

II. THEORETICAL MODEL AND ANALYSIS

Three energy levels in sodium atoms (in a heat-pipe oven) are employed in the experiment [Fig. 1(a)]. The pulse laser beams are spatially aligned as shown in Fig. 1(b). The pumping laser beams E_1 (ω_1, $\mathbf{k}_1$, and Rabi frequency $G_{g,M}$) and E_1' (ω_1, $\mathbf{k}_1'$, $G_{g,M}'$) (having a small angle of 0.3°) are tuned to the transition $|0\rangle$ ($3S_{1/2}$) to $|1\rangle$ ($3P_{3/2}$), and E_1 propagates in the opposite direction of the weak probe field E_3 (ω_1, $\mathbf{k}_3$, $G_{p,M}$), where M denotes the magnetic quantum number of the lower state in transition. These three laser beams are from the same near-transform-limited dye laser (10-Hz repetition rate, 5-ns pulsewidth and 0.04 cm^{-1} linewidth) with the frequency detuning $\Delta_1 = \omega_{10} - \omega_1$, where ω_{10} is the atomic transition frequency between $|0\rangle$ and $|1\rangle$. E_1 and E_1' (both with frequency ω_1) in beams 1 and 2 induce a population grating between states $|0\rangle$ and $|1\rangle$, which is probed by beam 3 (E_3) with the same frequency (ω_1). This interaction generates a DFWM signal E_f [Fig. 1(a)] satisfying the phase-matching condition [11]: $\mathbf{k}_f = \mathbf{k}_3 + \mathbf{k}_1 - \mathbf{k}_1'$. Then, an additional dressing field E_2 (ω_2, $\mathbf{k}_2$, $G_{d,M}$) is applied to the transition between $|1\rangle$ and the third level $|2\rangle$ ($4D_{3/2,5/2}$) with a frequency detuning $\Delta_2 (= \omega_{21} - \omega_2)$. E_2 is from another similar dye laser. Two quarter-wave plates (QWP) are used for changing the polarizations of the pumping fields $\mathbf{k}_1$, $\mathbf{k}_1'$. The generated DFWM signal is split into two equal components by a 50% beam splitter before detection, one is detected directly (denoted as I_T) and the other is further decomposed into P- and S-polarized components by a polarized beam splitter (PBS), which are denoted as I_P and I_S, respectively.

Figure 1(c) depicts the dressed-state picture with split $3P_{3/2}$ Zeeman sublevels, which corresponds to the DFWM suppression case when fields $\mathbf{k}_3$, $\mathbf{k}_1$, $\mathbf{k}_1'$ are on resonance with transition $|0\rangle \rightarrow |1\rangle$. Figure 1(d) shows the enhancement case when these fields are tuned to near the dressed energy level. For most cases in this work, only one QWP is used to modify the polarization state of $\mathbf{k}_1$, so it can be decomposed into linearly and circularly polarized components while all other fields are kept as linearly polarized [Fig. 1(a)]. In fact, we assume P-polarization direction as the quantization axis and the component perpendicular to it (S polarization) is decomposed into balanced left- and right-circularly polarized parts, while the component parallel to it (P polarization) keeps linearly polarized. Then the generated FWM signals will also contain linearly and circularly polarized components denoted as I_L and I_C, and they associate the detected intensities in the P and S polarizations with the equations, namely the detected intensities of I_P, I_S, and total intensity I_T in the

*ypzhang@mail.xjtu.edu.cn
†mxiao@uark.edu

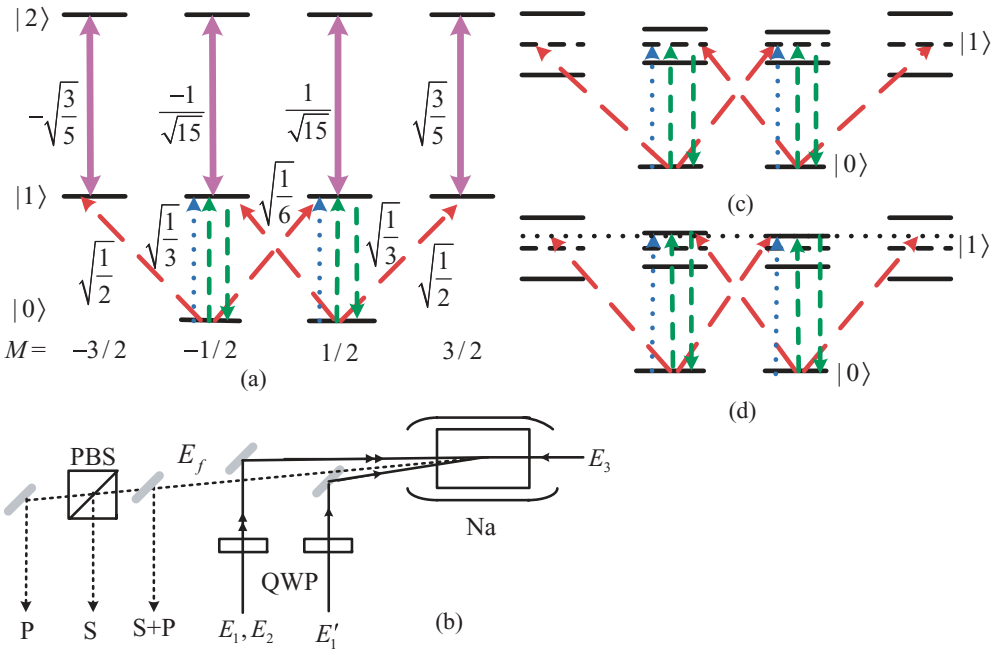

FIG. 1. (Color online) (a) Zeeman structure of the three-level ladder-type atomic system in the experiment and various transition pathways in it. Solid line, dressing field G_d; short-dashed lines, when the pumping fields are linearly polarized, G_g, G_g'; long-dashed lines, when the pumping fields are circularly polarized; dotted line, the probe field G_p. (b) The schematic diagram of the experiment. (c) and (d) Schematic diagrams for suppression and enhancement of the DFWM in the dressed-state picture.

real experiment can be written as: $I_P = I_L \cos^2\alpha + I_C/2$, $I_S = I_L \sin^2\alpha + I_C/2$, and $I_T = I_S + I_P = I_L + I_C$, where α is the angle between the P polarization and the direction of the linearly polarized signal. Since the CG coefficients may be different for different transitions between Zeeman sublevels, the Rabi frequencies are different even with the same laser field [7]. For example, considering CG coefficient values [12], we can obtain $|G^{\pm}_{g,\pm 3/2}|^2/|G^{\pm}_{g,\pm 1/2}|^2 = 3$, which indicates that the circularly polarized DFWM signal is mainly dressed by $G^0_{d,\pm 3/2}$, not by $G^0_{d,\pm 1/2}$. And also from CG coefficients, we can obtain that $|G^0_{d,\pm 3/2}|^2 = 9|G^0_{d,\pm 1/2}|^2$, which indicates that the dressing effects in the circularly polarized subsystems are far greater than in the linearly polarized subsystems.

Based on the discussion above, we can get the expressions for I_L and I_C. As Fig. 1(a) shows, there are two linearly polarized subsystems $[|0_M\rangle \overset{G^0_{g,M},(G^0_{g,M})^*,G^0_{p,M}}{\longleftrightarrow} |1_M\rangle\ (M = \pm 1/2)]$ that can generate linearly polarized DFWM, and are dressed by the linearly polarized dressing transition with $|G^0_{d,\pm 1/2}|^2$. By simply substituting the corresponding dressing terms into Eq. (4) of Ref. [13], we can obtain an expression of the density-matrix element, which induces the FWM signal of the linearly polarized component. To simplify the expression, the symmetry of CG coefficients is considered, namely $|G^0_{p(g,d)_M}| = |G^0_{p(g,d)_{-M}}|$ and $|G^+_{p(c,d)_M}| = |G^-_{p(c,d)_{-M}}|$. Moreover, if $G^{0,\pm}_{p(c,d)_M} \gg \Gamma_{0(1,2),0(1,2)}$, we can have the conditions of $\Gamma_{0(1,2),0(1,2)} \approx \Gamma_{0_M(1_M,2_M),0_M(1_M,2_M)}$. Consequently, the simplified expression is given by: $\rho^{(3)}_L = -2i|G^0_{gM}|^2 G^0_{pM}(A_1 + 2A_2)[1/(A_7 + A_3)^2 + 1/(\Delta_1^2 + \Gamma_{10}^2 + |G_{dM}|^4/A_4 + 2A_5|G_{dM}|^2/A_6)]$, where $A_1 = 1/\Gamma_{00} + 1/\Gamma_{11}$, $A_2 = \Gamma_{21}|G_{dM}|^2/(\Delta_2^2 + \Gamma_{21}^2)$, $A_3 = |G_{dM}|^2/[i(\Delta_1 + \Delta_2) + \Gamma_{21}]$, $A_4 = (\Delta_1 + \Delta_2)^2 + \Gamma_{21}^2$, $A_5 = -\Delta_1\Delta_2 - \Delta_1^2 + \Gamma_{10}\Gamma_{20}$, $A_6 = (\Delta_1 + \Delta_2)^2 + \Gamma_{20}^2$, and $A_7 = i\Delta_1 + \Gamma_{10}$.

On the other hand, the circularly polarized subsystems are more complicated [7,13]. In addition, besides being dressed by $|G^0_{d,\pm 1/2}|^2$, they are also dressed by $|G^0_{d,\pm 3/2}|^2$. Also, by inserting the dressing terms into Eq. (6) of Ref. [13] and under the same simplified conditions, we can obtain the expression of the density-matrix element, which induces the FWM signal of the circularly polarized component as: $\rho^{(3)}_C = -2B_1/[\Gamma_{00}(A_7 + B_2)^2] - \sum_{M=\pm 1/2} 2B_3/[\Gamma_{00}(A_7 + |G^0_{d_M}|^2/A_8)(A_7 + |G^0_{d_{M+1}}|^2/A_8)]$, where $A_8 = i(\Delta_1 + \Delta_2) + \Gamma_{20}$, $B_1 = iG^0_{p_{-1/2}} G^+_{g_{-1/2}} (G^0_{g_{-1/2}})^*$, $B_2 = |G^0_{d_{-1/2}}|^2/A_8$, and $B_3 = iG^0_{p_M}(G^0_{g_M})^* G^+_{g_M}$. Therefore, the intensities of the FWM in the P- and S-polarization directions are $I_L \propto |\rho^{(3)}_L|^2$ and $I_C \propto |\rho^{(3)}_C|^2$, respectively.

III. EXPERIMENTAL RESULTS

In the ladder-type three-level system (with Zeeman sublevels), as shown in Fig. 1(a), the pumping fields E_1 and E_1' (with diameter of 0.8 mm and power of 3 μW) and the probe field E_3 (with a diameter of 0.8 mm and power of 5 μW) are tuned to the line center (589.0 nm) of the lower $|0\rangle$ to $|1\rangle$ transition, which generate the DFWM signal E_f at frequency ω_1 by using one photon each from fields E_1, E_1', and E_3. The dressing field E_2 (with a diameter of 1.1 mm and power of 100 μW) scans from 568.5 to 569.1 nm (a crossing the upper $|1\rangle$ to $|2\rangle$ transition) to dress the DFWM process.

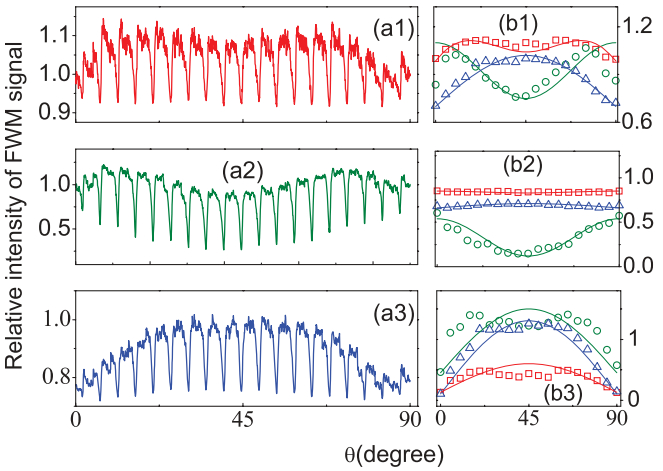

FIG. 2. (Color online) Polarization dependence of the suppressed DFWM signals. (a1)–(a3) Variations of I_T, I_P, and I_S (by scanning Δ_2) versus rotation angle $\theta(0°$–$90°$ per $5°)$, respectively. (b1)–(b3) Dependence curves of the background, minimums of the dips, and suppression depths for I_T (squares), I_P (circles), and I_S (triangles), respectively. The solid curves in (b1)–(b3) are the corresponding theory results; $\Delta_1 = 0$.

The suppression and enhancement of the DFWM processes happen as the probe field is set at different frequency detuning conditions. For example, when $\Delta_1 = 0$ [Fig. 1(c)], the DFWM signal is suppressed by the dressing field. For clearly understanding the influences of the incident beams to suppression and enhancement of FWM processes, we investigate the signals in P and S polarizations separately while the total intensity is the sum of intensities in these two polarizations components, as shown in Figs. 2(a1)–2(a3). The background represents the signal strength of the pure DFWM with no dressing field while the dips represent that the signal was suppressed at different polarizations of the pumping beam. When Δ_1 gets large enough [as in Fig. 1(d)], the DFWM signal is enhanced by the dressing field, as shown in Figs. 3(a1)–3(a3) and Figs. 3(d1)–3(d3). When Δ_1 is set at a proper position, which is not too far from the resonant position, both suppression (dips lower than background) and enhancement (peaks higher than background) can occur at the same time, as shown in Figs. 4(a1)–4(a3). The linewidths of the measured suppressed dips and enhanced peaks of FWM spectra are about 20 GHz.

Let us first consider the experimental results of the DFWM suppression. Figures 2(a1)–2(a3) present the DFWM spectra (with scanned dressing field Δ_2) from $\theta = 0$ to $\theta = 90°$ per $5°$, which is the polarization angle of the pumping field E_1. The dips below the background represent the suppressed DFWM by the dressing field. Figures 2(b1)–2(b3) present the θ-dependence curves of the background, the minimum of the suppressed dips, and depth of the suppressed dips (background minus minimum) in Figs. 2(a1)–2(a3), respectively. The dressing effect is clearly revealed by Fig. 2(b3), which shows that the suppression depths in P and S polarizations are both ascending as the QWP is rotated from $0°$ to $45°$. This can be explained by changing the DFWM subsystems from linearly polarized ones to circularly polarized ones, and then calculating the intensities I_P, I_S, and I_T. In fact, as Figs. 2(a1)–2(a3) show, DFWM signals are mainly generated in the linearly polarized subsystems that are dressed by $G^0_{d,\pm 1/2}$ when k_1 is linearly polarized ($\theta = 0$). As QWP is rotated, the linearly polarized transitions gradually transform into circularly polarized ones, which then involve the dressing transitions $G^0_{d,\pm 3/2}$ partly instead of $G^0_{d,\pm 1/2}$. Consequently, the dressing effect gets larger and the suppression dips become deeper as QWP is rotated from $0°$ to $45°$. Furthermore, the suppression condition ($\Delta_1 + \Delta_2 = 0$) for DFWM in all the subsystems is uniform because it contains no term relating to the Zeeman structure, which results in the similar dependence curves for S and P polarizations, as well as the total intensity, as shown in Figs. 2(a1)–2(a3).

Figure 2(b1) presents the polarization dependence of the background as well as the pure DFWM. The shapes of the curves for the P and S polarizations and the total intensity basically follow the well-expected classical

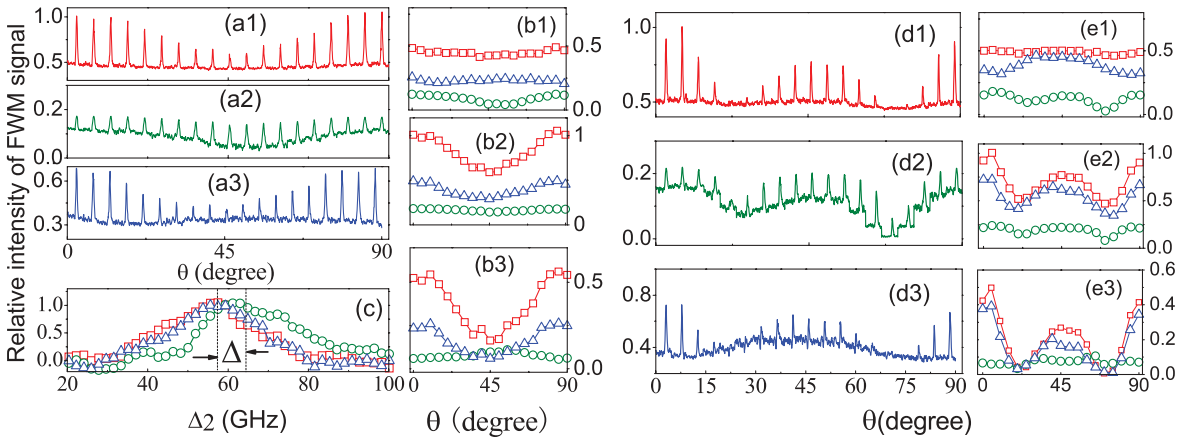

FIG. 3. (Color online) Polarization dependence of DFWM enhancement versus θ. (a1)–(a3) and (b1)–(b3) DFWM enhancement with conditions parallel to Fig. 2 except at $\Delta_1 = -67$ GHz. (c) I_P with scanning Δ_2 for $\theta = 0°$ (squares), $45°$ (circles), and $90°$ (triangles), when $\Delta_1 = 67$ GHz. (d1)–(d3) and (e1)–(e3) are for I_T, I_P, and I_S polarization dependencies, respectively, when both polarizations of the $\mathbf{k}_1$ and $\mathbf{k}'_1$ beams are rotated simultaneously, with $\Delta_1 = -67$ GHz.

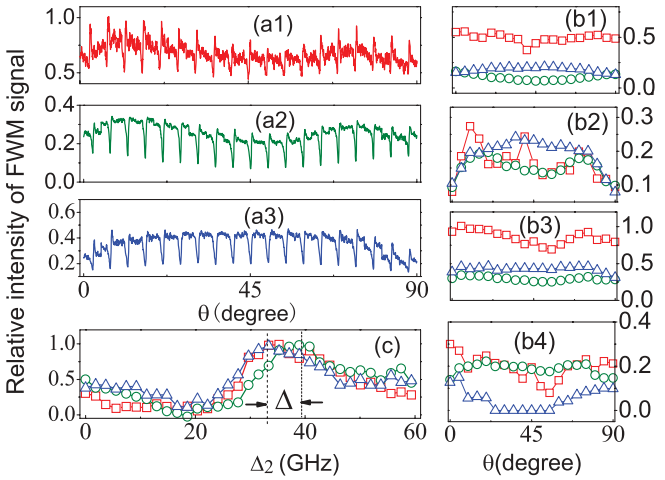

FIG. 4. (Color online) Polarization dependence of DFWM versus the rotation angle θ. (a1)–(a3) Half-enhancement and half-suppression with the condition parallel to Figs. 2(a1)–2(a3) except $\Delta_1 = -30$ GHz. (b1) and (b2) Dependencies of the minimum and maximum of each part on θ, (b3) depths of the suppressed dips, and (b4) heights of the enhanced peak for I_T (squares), I_P (circles), and I_S (triangles), respectively. (c) I_P as scanning Δ_2 for 0° (squares), 45° (circles), and 90° (triangles).

polarization spectroscopy [5,6]. Figure 2(b2) shows the polarization dependence of the dressed DFWM signal peak values, which include the pure DFWM and the suppression dips.

For DFWM enhancement when $\mathbf{k}_3$, $\mathbf{k}_1$, $\mathbf{k}_1'$ are far detuned [Fig. 1(d)], as shown in Fig. 3, the polarization dependence of the enhanced peak heights (maximum minus background) for the S polarization is different [Fig. 3(b3) triangle points]: it descends as QWP is rotated from 0° to 45°. Comparing expressions of I_L and I_C above, we can see that at far detuning condition for $\mathbf{k}_3$, $\mathbf{k}_1$, $\mathbf{k}_1'$, the polarization variation of $\mathbf{k}_1$ enlarges α. It means that S- polarized components projecting from linearly polarized FWM are increasing while P-polarization components are decreasing gradually as rotating QWP. Consequently, the dressing efficiency of the S polarization is relatively reduced as compared with the condition when $\mathbf{k}_1$ is linearly polarized. On the other side, the P-polarization component is relatively enhanced.

As discussed above, the dressing field Rabi frequencies for different Zeeman sublevels may be different (e.g., $|G^0_{d,\pm 3/2}|^2 = 9|G^0_{d,\pm 1/2}|^2$), which will induce different splitting distances for different sublevels. The exact expression of the split sublevel positions are $\delta_M = (\Delta_2 \pm \sqrt{\Delta_2^2 + 4|G_{dM}|^2})/2$. The enhanced peaks appear when the splitting sublevels are on resonance with the generating fields G_g, G_g', and the probe field G_p. This then satisfies the enhancement condition $\Delta_1 + \delta_M = 0$ [14]. Combining it with $\delta_M = (\Delta_2 \pm \sqrt{\Delta_2^2 + 4|G_{dM}|^2})/2$, we can obtain the positions of the enhanced peaks in the plotted figure: $O_M = (\Delta_1^2 - |G^0_{d,M}|^2)/\Delta_1$. There should be two distinct enhanced peaks $O_{\pm 3/2}$ and $O_{\pm 1/2}$, which are covered in the wide power-broadened profile. However, when $\mathbf{k}_1$ is linearly ($\theta = 0$) and circularly ($\theta = 45°$) polarized, the enhanced peaks are primarily created by $M = \pm 1/2$ and $M = \pm 3/2$, which are at $O_{\pm 1/2}$ and $O_{\pm 3/2}$, respectively, as shown in Fig. 3(c). By using O_M expression and the CG coefficients, we can calculate the shift distance between the enhanced peaks as: $\Delta = O_{3/2} - O_{1/2} = (|G^0_{d,3/2}|^2 - |G^0_{d,1/2}|^2)/\Delta_1 \approx 8.8$ GHz. The measured shift distance between the enhanced peaks in Fig. 3(c) is about 7.5 GHz.

When two QWPs are used to change the polarizations of the $\mathbf{k}_1$ and $\mathbf{k}_1'$ beams simultaneously, as shown in Figs. 3(d1) and 3(d2). The variation period is reduced to half of the case with changing $\mathbf{k}_1$ only. Also, the enhancement peak gets close to 0 at about $\theta = 22.5°$.

Finally, we set the frequency detuning of $\mathbf{k}_3$, $\mathbf{k}_1$, $\mathbf{k}_1'$ at an intermediate position (about 30 GHz, smaller than the value in the enhancement case), half-enhancement and half-suppression appear when the frequency of the dressing field is scanned [11], which is also modified by the polarization variation of $\mathbf{k}_1$, as shown in Fig. 4. The variation rules also follow the ones discussed above: the background obeys traditional laws [5,6], the dependencies of the suppression and enhancement curves on the polarization are similar to the results in suppression (Fig. 2) and enhancement (Fig. 3) parts, respectively.

IV. CONCLUSION

In summary, we have reported our experimental results about the evolutions of dressed DFWM effects when the polarizations of the pumping fields are changed. In the suppressed DFWM case, the generated DFWM signals in P and S polarizations are both ascending as the QWP changes from 0° to 45°, which is caused by different dressing strengths for the linearly polarized and circularly polarized DFWM signals. In the enhanced DFWM case, the dependence curve for the S-polarized DFWM signal descends while the P-polarization component ascends as the QWP is rotated. The experimentally measured data are in good agreements with the results from dressed-state analysis involving all relevant Zeeman sublevels. In addition, the dressing effects strongly depend on the dipole moments of the transitions, which can provide an easy and qualitative way to determine the orders of magnitude of the effective dipole moments for different transitions by measuring the shifted distances between two enhanced peaks when the pump field's polarization is changed. Such studies provide detail physical mechanisms to control and optimize the efficiencies of the multiwave mixing processes in multilevel atomic systems.

ACKNOWLEDGMENTS

This work was supported by the National Natural Science Foundation of China (Grant No. 10974151), the New Century Excellent Talent Project of the Ministry of Education of China (Grant No. 08-0431), and the Cross-Disciplinary Project of Xi'an Jiaotong University (Grant No. 2009xjtujc08).

[1] S. E. Harris, Phys. Today **50**, 36 (1997).
[2] J. Gea-Banacloche, Y. Q. Li, S. Z. Jin, and M. Xiao, Phys. Rev. A **51**, 576 (1995).
[3] B. Wang, Y. J. Xiao, X. Yang, C. Xie, H. Wang, and M. Xiao, Opt. Lett. **31**, 3647 (2006).
[4] M. A. Yuratich and D. C. Hanna, J. Phys. B **9**, 729 (1976).
[5] C. J. Zhu, A. A. Senin, Z. H. Lu, J. Gao, Y. Xiao, and J. G. Eden, Phys. Rev. A **72**, 023811 (2005).
[6] W. C. Magno, R. B. Prandini, P. Nussenzveig, and S. S. Vianna, Phys. Rev. A **63**, 063406 (2001).
[7] H. B. Zheng, Y. P. Zhang, U. Khadka, R. M. Wang, C. B. Li, Z. Q. Nie, and M. Xiao, Opt. Express **17**, 15468 (2009).
[8] H. Y. Ling, Y. Q. Li, and M. Xiao, Phys. Rev. A **53**, 1014 (1996).
[9] S. Li, B. Wang, X. Yang, Y. Han, H. Wang, M. Xiao, and K. C. Peng, Phys. Rev. A **74**, 033821 (2006).
[10] C. B. Li, H. B. Zheng, Y. P. Zhang, Z. Q. Nie, J. P. Song, and M. Xiao, Appl. Phys. Lett. **95**, 041103 (2009).
[11] Y. Zhang, B. Anderson, A. W. Brown, and M. Xiao, Appl. Phys. Lett. **91**, 061113 (2007).
[12] Y. G. Du, Y. P. Zhang, C. C. Zuo, C. B. Li, Z. Q. Nie, H. B. Zheng, M. Z. Shi, R. M. Wang, J. P. Song, K. Q. Lu, and M. Xiao, Phys. Rev. A **79**, 063839 (2009).
[13] R. M. Wang, Y. G. Du, Y. P. Zhang, H. B. Zheng, Z. Q. Nie, C. B. Li, Y. Y. Li, J. P. Song, and M. Xiao, J. Opt. Soc. Am. B **26**, 1710 (2009).
[14] Z. C. Zuo, J. Sun, X. Liu, Q. Jiang, G. Fu, L. A. Wu, and P. M. Fu, Phys. Rev. Lett. **97**, 193904 (2006).